JM PAPERS

Opposite effects of a reaction-driven viscosity decrease on miscible viscous fingering depending on the injection flow rate

R.X. Suzuki[1], S. Arai[1], T. Masumo[1], Y. Nagatsu[1] and A. De Wit[2],†

[1]Department of Chemical Engineering, Tokyo University of Agriculture and Technology, Naka-cho 2-24-16, Koganei, Tokyo 184-8588, Japan

[2]Nonlinear Physical Chemistry Unit, Université libre de Bruxelles (ULB), CP231, Faculté des Sciences, Campus Plaine, 1050 Brussels, Belgium

When a less-viscous solution of a reactant A displaces a more-viscous solution of another reactant B, a fast bimolecular $A + B \rightarrow C$ reaction decreasing locally the viscosity can influence the viscous fingering (VF) instability taking place between the two miscible solutions. We show both experimentally and numerically that, for monotonic viscosity profiles, this decrease in viscosity has opposite effects on the fingering pattern depending on the injection flow rate. For high flow rates, the reaction enhances the shielding effect, creating VF patterns with a lower surface density, i.e. thinner fingers covering a smaller area. In contrast, for lower flow rates, the reaction stabilises the VF dynamics, i.e. delays the instability and gives a less-deformed displacement, reaching in some cases an almost-stable displacement. Nonlinear simulations of reactive VF show that these opposite effects at low or high flow rates can only be reproduced if the diffusivity of A is larger than that of B, which favours a larger production of the product C and, hence, a larger viscosity decrease. The analysis of one-dimensional viscosity profiles reconstructed on the basis of a one-dimensional reaction–diffusion–advection model confirms that the VF stabilisation at low Péclet number and in the presence of differential diffusion of reactants originates from an optimum reaction-driven decrease in the gradient of the monotonic viscosity profile.

Key words: fingering instability, Hele-Shaw flows, laminar reacting flows

1. Introduction

The displacement of one fluid by another in porous media is commonly encountered in environmental and industrial flows. When the injected fluid is more viscous than the

† Email address for correspondence: anne.de.wit@ulb.be

displaced one, the displacement is hydrodynamically stable and the interface between both fluids remains planar. In the reverse situation where the invading fluid is less viscous than the displaced one, the interface shows a finger-like deformation because the interface is hydrodynamically unstable with regard to a viscous fingering (VF) instability (Engelberts & Klinkenberg 1951; Saffman & Taylor 1958; Homsy 1987). VF with or without chemical reactions has been well studied so far (Homsy 1987; McCloud & Maher 1995; De Wit 2020) because of its wide range of applications such as in transport of digestive juices (Bhaskar *et al.* 1992), chromatography (Broyles *et al.* 1998; Haudin *et al.* 2016), secondary and ternary oil recovery (Lake *et al.* 2014; Sabet *et al.* 2020) and CO_2 sequestration (Berg & Ott 2012) to name a few. In the miscible displacement of a solution of *B* of viscosity μ_b by a solution of *A* of viscosity μ_a, an important parameter controlling VF is the log-mobility ratio $R_b = \ln(\mu_b/\mu_a)$. If $R_b > 0$, the displacement is unstable and VF is all the more vigorous if R_b is increased or the flow rate is larger (Homsy 1987). The $R_b < 0$ case is stable, leading to stable planar interfaces in non-reactive systems.

Fingering patterns can be modified by reactions which change viscosity, permeability or interfacial tension (Nagatsu 2015; De Wit 2016, 2020). Experiments have provided evidence for, for example, changes in the fingering pattern due to a decrease in interfacial tension induced by a reaction in immiscible systems (Fernandez & Homsy 2003; Tsuzuki *et al.* 2019) or due to a decrease in permeability by a precipitation reaction in miscible systems (Nagatsu *et al.* 2008, 2014; Haudin & De Wit 2015; Shukla & De Wit 2016). When a chemical reaction affects the VF dynamics, the value of the dimensionless Damköhler number D_a defined as the ratio of the characteristic time of advection to that of the chemical reaction is an additional important parameter.

From a theoretical point of view, miscible reactive VF for which the reaction induces *in situ* a change in viscosity has been investigated numerically in the case of a bistable chemical reaction changing the viscosity across a moving chemical front, inducing a new mechanism of 'droplet' formation (De Wit & Homsy 1999). Later, linear stability analysis (Hejazi *et al.* 2010; Kim *et al.* 2021) and nonlinear simulations (Gérard & De Wit 2009; Nagatsu & De Wit 2011; Sharma *et al.* 2019; Kim *et al.* 2021; Tafur *et al.* 2021; Verma, Sharma & Mishra 2022) have classified the stabilising or destabilising influence of simple $A + B \rightarrow C$ reactions on VF. For such simple bimolecular reactions, an important parameter is the log-mobility ratio $R_c = \ln(\mu_c/\mu_a)$ comparing the viscosities of equimolar solutions of the product *C* or reactant *A*. Most theoretical works on this reactive VF have considered the case where the initial concentration of *A* and *B* is the same and all species diffuse at the same rate. Under this condition, if $R_c = R_b$, the product has the same viscosity as the reactant *B* and the reactive case is exactly the same as the non-reactive one. If $R_c < R_b$, the reaction decreases the viscosity while viscosity increases if $R_c > R_b$. As long as $0 < R_c < 2R_b$, the viscosity profile remains monotonic. An extremum in viscosity is observed if $R_c < 0$ or $R_c > 2R_b$. When $R_b < 0$ and there is an extremum in viscosity, modelling predicts that, similarly to differential diffusion effects (Mishra *et al.* 2010), reactions are able to destabilise otherwise stable displacements thanks to the build-up of non-monotonic viscosity profiles (Hejazi *et al.* 2010; Nagatsu & De Wit 2011; Riolfo *et al.* 2012; Escala *et al.* 2019).

In 2007, Nagatsu *et al.* (2007) reported the first experimental study of miscible VF with viscosity changes induced by a very fast chemical reaction (infinite D_a) during a radial injection in a Hele-Shaw cell. In this study, polymer solutions with viscosity depending on pH were displaced by less-viscous acid or base aqueous solutions ($R_b > 0$ case). The reaction modifies locally the gradient in viscosity but the viscosity profile remains monotonically increasing. It was shown that, at fixed large flow rates, reactive

VF patterns have a larger surface density, i.e. cover a larger area than their non-reactive equivalent at given times and flow rates when the reaction increases the viscosity. This is due to the fact that the reaction widens the fingers and decreases the shielding effect. In contrast, in the case of a decrease in viscosity by reaction, the surface density of the VF patterns is lower, i.e. fingers are thinner and shielding is enhanced. Subsequently, similar reactive VF experiments with monotonic increasing viscosity profiles have been performed under moderate D_a conditions using slower reactions for both chemically driven viscosity decrease (Nagatsu *et al.* 2009) and increase (Nagatsu *et al.* 2011). It was shown that, for such intermediate D_a conditions, the experimental results were opposite to those of the infinite D_a case, i.e. the area occupied by the VF pattern was increased (decreased) in case of viscosity decrease (increase).

In the case of reactive VF ($R_b > 0$) with non-monotonic viscosity profiles featuring a maximum, experiments have shown that the maximum induces fingers extending preferentially towards the back of the reaction zone (Bunton *et al.* 2017). By increasing experimentally the Damköhler number, the stabilising effect of the reaction can as well be enhanced (Stewart *et al.* 2018). The reactive destabilisation of an otherwise stable front ($R_b < 0$) has been achieved experimentally in the case of the reactive displacement of acid or base aqueous solutions by a more-viscous polymer solution showing that the chemically induced pattern is different depending on whether the reaction builds a maximum or a minimum (Riolfo *et al.* 2012). Destabilisation induced by a pH sensitive clock reaction has also shown how the reactive feedback of a pH-changing reaction on viscosity can control fingering (Escala *et al.* 2019; Escala & Munuzuri 2021). The destabilisation of the case of reactant solutions of same viscosities, i.e. $R_b = 0$ has been studied experimentally by Podgorski *et al.* (2007).

Numerical simulations of reactive miscible VF with viscosity changes by an instantaneous $A + B \rightarrow C$ chemical reaction for infinite D_a conditions (Nagatsu & De Wit 2011) and variable R_b and R_c are in good agreement with the experimental results (Nagatsu *et al.* 2007), i.e. an increase (decrease) of viscosity by the reaction leads to surface denser (less-dense) VF patterns. For $R_b = 0$, the effect on the properties of reactive fingering of varying the Damköhler number, the contrast in viscosity between products and reactant, the initial concentrations, and the diffusion coefficients (Gérard & De Wit 2009; Verma *et al.* 2022) are in good agreement with the experiments from Podgorski *et al.* (2007). In particular, Gérard & De Wit (2009) showed that, even if the solutions of the two reactants A and B have the same viscosity, the VF pattern is different whether A is injected into B or the reverse as soon as these reactants have different diffusion coefficients or different initial concentrations because the underlying concentration profiles controlling the viscosity profile are not symmetric. This study was however limited to the case $R_b = 0$ and did not investigate the effect of changing the value of *Pe*.

The effect of varying the Péclet number has been investigated numerically as well, showing that, as expected, decreasing *Pe* for non-reactive cases stabilises VF (Homsy 1987; Pramanik & Mishra 2015; Shukla & De Wit 2020). Interestingly, Hejazi & Azaiez (2010) show that, for $A + B \rightarrow C$ reactions with moderate D_a, larger *Pe* can lead to slower rates of chemical production, i.e. less product C generated at a same time. This is attributed to the fact that the mixing between reactants by diffusion is then less efficient at early times. Shukla & De Wit (2020) have performed a numerical study of the effect of $A + B \rightarrow C$ reactions on VF when varying *Pe* for a finite D_a and equal diffusion coefficients, focusing on the case of a viscosity-decreasing reaction both in the case of monotonic and non-monotonic viscosity profiles. They found that the viscosity-decreasing reaction has an increased stabilising effect when *Pe* is decreased in the sense that the
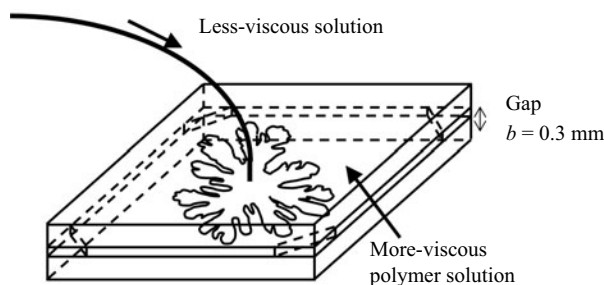
Figure 1. Schematic of the Hele-Shaw cell reactor.

mixing length of species A at given times is smaller in the reactive case than that in the non-reactive one when Pe is lower. This effect was attributed to a build-up of a minimum in the viscosity profile. However, the mixing lengths of species B and C at given times in the reactive case were larger than those in the non-reactive case and the study focused on equal diffusion coefficients only.

It is of interest to study to what extent overall stabilisation can also be obtained for monotonic profiles and what is the role of differential diffusion effects. Moreover, experiments on miscible VF with $A + B \rightarrow C$ reactions for which the Péclet number is varied in a wide range are not yet available.

In this context, we have experimentally investigated the influence of changes in the injection flow rate or, equivalently, changes in the Péclet number Pe on miscible VF when a bimolecular $A + B \rightarrow C$ reaction decreases viscosity. In the experiments, we analyse the change in the VF patterns when viscous polymer solutions are displaced by a less-viscous acidic solution such that the viscosity is decreased *in situ* via reaction-driven pH changes. Scanning a wide range of flow rates, we show that this reaction-driven viscosity decrease has opposite effects on the VF pattern at high and low flow rates, respectively. Interestingly, for lower flow rates, a full stabilisation of the interface by reaction is obtained. In parallel, a numerical investigation of the influence of changes in the Péclet number Pe on VF for a viscosity decreasing reaction with monotonic viscosity profiles confirms the same trend provided the injected reactant diffuses sufficiently faster than the displaced one. Our findings pave the way to devise a control of VF by chemical reactions choosing suitable reactants and flow conditions.

2. Experimental set-up and numerical description

2.1. *Experimental set-up*

Experiments are conducted in a horizontal Hele-Shaw cell consisting in two glass plates separated by a thin gap in which a viscous fluid is displaced by another less-viscous one, injected through a central hole at a fixed flow rate (see figure 1). The gap of the cell b is fixed to 0.3 mm and the injection flow rate q is varied from 9.2×10^{-11} to 3.6×10^{-8} m^3 s^{-1}. In reactive displacements, the displaced more-viscous solution is a 0.125 wt % sodium polyacrylic acid (SPA) solution (molecular weight of 2.1–6.6×10^6) while the injected displacing less-viscous fluid is a 0.2 M HCl aqueous solution. Upon contact between these solutions, a chemical reaction produces polyacrylic acid (PAA), resulting in a viscosity decrease at an instantaneous rate (Nagatsu *et al.* 2007, 2010).

For the non-reactive case, the same 0.125 wt % SPA solution and deionised water are used as the more- and less-viscous solutions, respectively. In all cases, the less-viscous
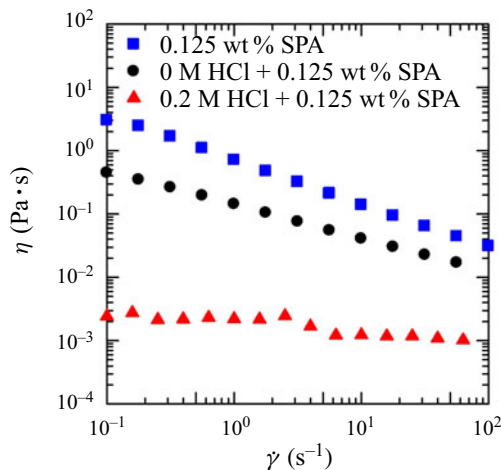
Figure 2. Viscosity as a function of shear rate of the more-viscous fluid (blue squares) and that of the solution obtained by mixing equal volumes of a 0.125 wt % SPA solution and of a solution of 0 M (black circles) or 0.2 M HCl (red triangles) including 0.1 wt % trypan blue.

solutions are dyed with trypan blue for visualisation of the dynamics. The viscosity of the various fluids was measured using a commercial viscosimeter (from TA Instruments, Japan). The viscosity of the more-viscous polymer solution is shear thinning, i.e. decreases with the shear rate as shown by the blue squares in figure 2. The viscosities of the displacing dyed Newtonian 0.2 M HCl aqueous solution or pure water are 1.1 and 1.0 mPa·s, respectively. We also measured the viscosity of a mixture of equal volumes of 0.125 wt % SPA solution and 0.2 M HCl solution (in the reactive case) and that of 0.125 wt % SPA solution and water (in the non-reactive case), see figure 2. We find that the viscosity in the reactive mixture system is much lower than that in the non-reactive one and that the reaction, in effect, decreases the viscosity.

2.2. *Numerical simulations*

To simulate the experiments shown above, we consider a horizontal Hele-Shaw cell of length L_x and width L_y with constant permeability κ in which a miscible solution of reactant A with viscosity μ_A is injected from left to right into a polymer solution of reactant B with viscosity μ_B at a constant speed U along the x direction (figure 3). A bimolecular $A + B \rightarrow C$ reaction giving the product C with viscosity μ_C takes place in the contact zone between reactants A and B. Here, species A, B and C correspond to HCl, SPA and PAA, respectively in the experiment. As in experiments, we follow the dynamics by the spatiotemporal evolution of the neutral dye, E, initially dissolved in the injected solution. We assume that buoyant effects are negligible and that the fluids are incompressible. The dynamics is described by Darcy's law coupled to reaction–diffusion–advection equations for the concentrations:

$$\nabla \cdot \boldsymbol{u} = 0, \tag{2.1}$$

$$\nabla p = -\frac{\mu(b, c)}{\kappa} \boldsymbol{u}, \tag{2.2}$$

$$\frac{\partial a}{\partial t} + \boldsymbol{u} \cdot \nabla a = D_A \nabla^2 a - kab, \tag{2.3}$$
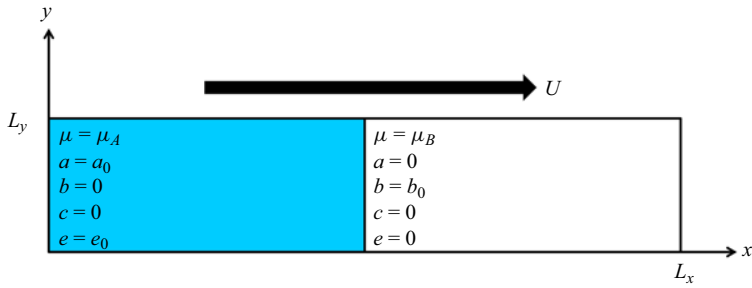
1001 A25-5

Figure 3. Two-dimensional porous medium of length L_x and width L_y with permeability κ in which a miscible solution of reactant A with viscosity μ_A is injected from left to right into a solution of reactant B with viscosity $\mu_B > \mu_A$ at a constant speed U along the x direction. Here, a_0, b_0 and e_0 are the initial concentration of reactant A, reactant B and dye E, respectively.

$$\frac{\partial b}{\partial t} + \boldsymbol{u} \cdot \nabla b = D_B \nabla^2 b - kab, \tag{2.4}$$

$$\frac{\partial c}{\partial t} + \boldsymbol{u} \cdot \nabla c = D_C \nabla^2 c + kab, \tag{2.5}$$

$$\frac{\partial e}{\partial t} + \boldsymbol{u} \cdot \nabla e = D_E \nabla^2 e, \tag{2.6}$$

$$\mu(b, c) = \mu_A \exp\left(R_b \frac{b}{f_0} + R_c \frac{c}{f_0}\right), \tag{2.7}$$

where μ_A, μ_B and μ_C are the viscosities of the solutions of A, B and C at a same reference concentration f_0. Here a, b, c and e denote the concentrations of the reactants A and B, the product C and the dye E, respectively; $\boldsymbol{u} = (u, v)$ is the two-dimensional velocity; k is the kinetic constant; p is the pressure; D_I is the diffusivity coefficient of species I; $\mu(b, c)$ is the viscosity; R_b and R_c are the log-mobility ratio defined as

$$R_b = \ln\left(\frac{\mu_B}{\mu_A}\right), \quad R_c = \ln\left(\frac{\mu_C}{\mu_A}\right). \tag{2.8a,b}$$

Note that, except for (2.7), the formulation is equivalent to the model of Shukla & De Wit (2020). For the non-reactive case, the system is hydrodynamically unstable when the less-viscous solution of A displaces the more-viscous solution of B, i.e. when $\mu_A < \mu_B$ or $R_b > 0$. To mimic the fact that the reaction decreases viscosity in the experiments (see figure 2), we consider here $R_b = 2$ and $R_c = 0$ such that the product C is less viscous than the reactant B but we keep a monotonic viscosity profile.

2.3. *Non-dimensional equations*

To specifically let the Péclet number appear in the dimensionless problem, the reference scales for length, velocity, time, concentration, viscosity, diffusivity and pressure are taken as L_y, U, L_y/U, f_0, μ_A, D_C and $\mu_A U L_y/\kappa$, respectively. For simplicity, equations are written in a reference frame moving with speed U with $\boldsymbol{e_x}$ being the unit vector along

x direction. The dimensionless forms of (2.1)–(2.8*a*,*b*) can be written as

$$\nabla \cdot \boldsymbol{u} = 0, \tag{2.9}$$

$$\nabla p = -\mu(b, c)(\boldsymbol{u} + \boldsymbol{e_x}), \tag{2.10}$$

$$\frac{\partial a}{\partial t} + \boldsymbol{u} \cdot \nabla a = \frac{\delta_A}{Pe}\nabla^2 a - D_a ab, \tag{2.11}$$

$$\frac{\partial b}{\partial t} + \boldsymbol{u} \cdot \nabla b = \frac{\delta_B}{Pe}\nabla^2 b - D_a ab, \tag{2.12}$$

$$\frac{\partial c}{\partial t} + \boldsymbol{u} \cdot \nabla c = \frac{1}{Pe}\nabla^2 c + D_a ab, \tag{2.13}$$

$$\frac{\partial e}{\partial t} + \boldsymbol{u} \cdot \nabla e = \frac{\delta_E}{Pe}\nabla^2 e, \tag{2.14}$$

$$\mu(b, c) = \exp(R_b b + R_c c), \tag{2.15}$$

where $D_a = kf_0 L_y/U = \tau_h/\tau_c$ is the dimensionless Damköhler number defined as the ratio of the hydrodynamic time scale $\tau_h = L_y/U$ to the chemical time scale $\tau_c = 1/kf_0$. The Péclet number $Pe = UL_y/D_C = \tau_D/\tau_h$ is the ratio of the diffusive time $\tau_D = L_y^2/D_C$ and the advective time τ_h while $\delta_A = D_A/D_C$, $\delta_B = D_B/D_C$ and $\delta_E = D_E/D_C$ are the diffusion coefficient ratios (Shukla & De Wit 2020). Taking the curl of the momentum equation and defining the stream function ψ as $u = \partial\psi/\partial y$ and $v = -\partial\psi/\psi x$, we obtain

$$\nabla^2\psi = R_b\left(\frac{\partial\psi}{\partial x}\frac{\partial b}{\partial x} + \frac{\partial\psi}{\partial y}\frac{\partial b}{\partial y} + \frac{\partial b}{\partial y}\right) + R_c\left(\frac{\partial\psi}{\partial x}\frac{\partial c}{\partial x} + \frac{\partial\psi}{\partial y}\frac{\partial c}{\partial y} + \frac{\partial c}{\partial y}\right), \tag{2.16}$$

$$\frac{\partial a}{\partial t} + \frac{\partial\psi}{\partial y}\frac{\partial a}{\partial x} - \frac{\partial\psi}{\partial x}\frac{\partial a}{\partial y} = \frac{\delta_A}{Pe}\nabla^2 a - D_a ab, \tag{2.17}$$

$$\frac{\partial b}{\partial t} + \frac{\partial\psi}{\partial y}\frac{\partial b}{\partial x} - \frac{\partial\psi}{\partial x}\frac{\partial b}{\partial y} = \frac{\delta_B}{Pe}\nabla^2 b - D_a ab, \tag{2.18}$$

$$\frac{\partial c}{\partial t} + \frac{\partial\psi}{\partial y}\frac{\partial c}{\partial x} - \frac{\partial\psi}{\partial x}\frac{\partial c}{\partial y} = \frac{1}{Pe}\nabla^2 c + D_a ab, \tag{2.19}$$

$$\frac{\partial e}{\partial t} + \frac{\partial\psi}{\partial y}\frac{\partial e}{\partial x} - \frac{\partial\psi}{\partial x}\frac{\partial e}{\partial y} = \frac{\delta_E}{Pe}\nabla^2 e. \tag{2.20}$$

The initial conditions for the stream function and product concentration are taken as $\psi(x, y) = 0$ and $c(x, y) = 0$, for all (x, y). For the initial concentrations of the reactant A and B solutions, we use a step function between $a = 10$, $b = 0$ on the left and $b = 1$, $a = 0$ on the right of $x = x_0$ where x_0 is the initial position of the interface with a random noise of amplitude of order 10^{-2} added in the front to trigger the instability. To solve (2.16)–(2.20), we use a pseudo-spectral method based on Fourier coefficients (Tan & Homsy 1988; Gérard & De Wit 2009; Pramanik & Mishra 2015). The numerical domain has a size of 1024×256 for $Pe \leq 2000$ and 4096×1024 for $Pe = 4000$ and 8000. Boundary conditions are periodic in both directions. This is standard for the transverse direction and yields good results along the longitudinal direction as long as the length L_x is taken sufficiently long for the two fronts not to interact. Figures of the fingering dynamics focus on the unstable front.

Note that, for a given reference concentration f_0 and geometry, the diffusive and chemical time scales τ_d and τ_c are constant. Our simulations aim to investigate the effects
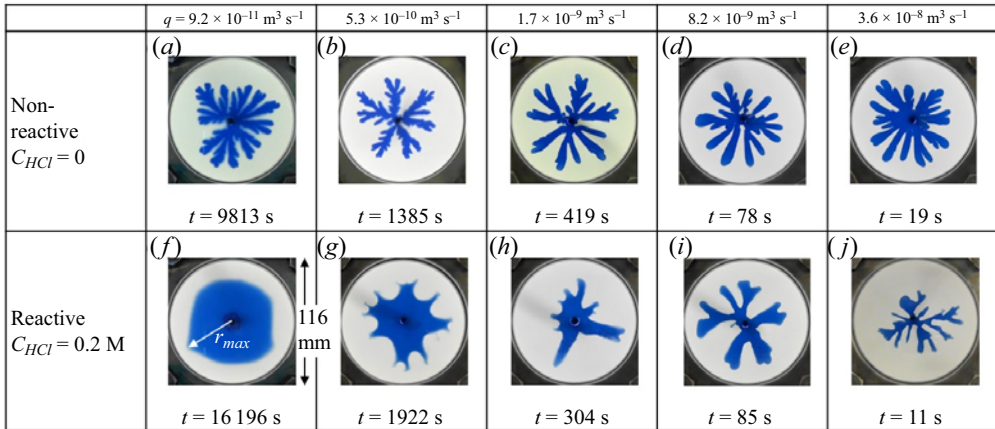
	$q = 9.2 \times 10^{-11}$ m³ s⁻¹	5.3×10^{-10} m³ s⁻¹	1.7×10^{-9} m³ s⁻¹	8.2×10^{-9} m³ s⁻¹	3.6×10^{-8} m³ s⁻¹
Non-reactive $C_{HCl} = 0$	(a) $t = 9813$ s	(b) $t = 1385$ s	(c) $t = 419$ s	(d) $t = 78$ s	(e) $t = 19$ s
Reactive $C_{HCl} = 0.2$ M	(f) r_{max} $t = 16\,196$ s	(g) 116 mm $t = 1922$ s	(h) $t = 304$ s	(i) $t = 85$ s	(j) $t = 11$ s

Figure 4. Displacement patterns comparing for different injection flow rates the non-reactive cases (upper line) and the reactive cases (bottom line) at the time (given in each panel) when the longest finger has reached the distance $r_{max} = 0.8 r_{HS}$ where $r_{HS} = 58$ mm is the radius of the cell.

of varying the flow rate. To do so, we vary U and hence Pe by changing τ_h. As $Pe = \tau_d/\tau_h$ and $D_a = \tau_h/\tau_c$, we have that $Pe \cdot Da = $ const. such that any change in Pe implies a change in D_a as well (Escala & Munuzuri 2021). Here, we fix $Pe \cdot Da = 8000$.

3. Results and discussion

3.1. *Displacement experiments*

Experimental results comparing unstable displacements with or without reaction are shown in figure 4. First, we see that, as expected, increasing the flow rate allows to reach the same position much faster in both cases. In the non-reactive case, especially at lower flow rates, the pattern features very branched fingers, similar to those observed in other non-Newtonian systems (Nittman, Daccord & Stanley 1985; Zhao & Maher 1992; Kawaguchi 2001). In contrast, in the higher-flow-rate regime, the dynamics is rather similar to those seen with Newtonian non-reactive fluids with less-branched patterns owing to the shear-thinning viscosity and the higher shear rate. Note that the sharpness of the viscosity profile along the gap direction may also play a role (Lajeunesse *et al.* 1997; Videbaek & Nagel 2019; Keable *et al.* 2022) as seen when, for instance, the colour becomes less intense around the fingertip (Videbaek & Nagel 2019; Keable *et al.* 2022). In our experimental results, the colour intensity of the dye is almost uniform over the whole VF pattern as shown in figures 4 and 7. Hence, we do not explore the three-dimensional structure of the fingers any further. This is also motivated by the fact that ratios of viscosities μ_B/μ_A are here typically of the order of 10^2–10^3 depending on flow rate and position along the radius so that we do not expect here to see patterns with proportionate growth as observed at lower viscosity ratios when flow rate is varied (Bischofberger, Ramachandran & Nagel 2014; Videbaek & Nagel 2019).

As seen qualitatively in figure 4 and quantitatively in figure 5 (see Appendix B for details on finger width measurements), the typical finger width does not depend much on the injection flow rate q for the non-reactive case. To understand this, we recall that, because of the shear thinning fluid property of the more-viscous fluid, its apparent viscosity and, hence, the viscosity contrast between the two solutions is decreasing with an increase in the flow rate. This stabilising effect is counterbalanced by the fact that, classically, an increase
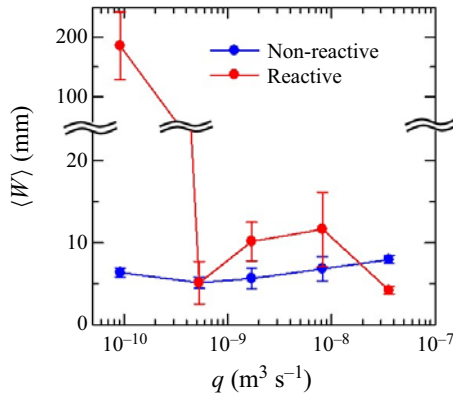
Figure 5. Average finger width $\langle w \rangle$ as a function of flow rate q for the patterns shown in figure 4. The error bars represent the standard deviation for experiments repeated at least three times.
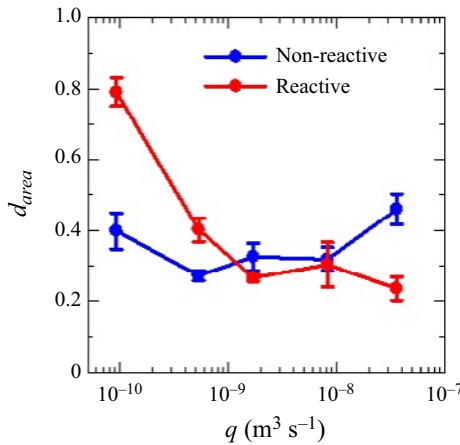

Figure 6. Area density, d_{area}, as a function of the flow rate q for the non-reactive and reactive cases of the patterns shown in figure 4. The error bars represent the standard deviation for experiments repeated at least three times.

in the flow rate increases the fingering destabilisation (Homsy 1987). Hence, the balance between both effects induces that the typical finger width of the non-reactive pattern is almost independent of the flow rate. Similar effects occur in VF of non-Newtonian immiscible fluids as well (Bonn *et al.* 1995; Singh, Lalitha & Mondal 2021).

A temporal evolution of both non-reactive and reactive patterns is shown at the lowest and highest q in figure 7. Note that the wavelength of the fingers at onset in the non-reactive case does not scale as $4b$ as seen in some studies (Paterson 1985), probably due to the non-Newtonian character of the displaced solution.

In the reactive case, in contrast, we see that while fingers form at higher flow rates, the displacement is stabilised at the lowest injection speed. Quantitatively, we measure that, when q increases, fingers typically become narrower and the VF patterns have a lower surface density than the non-reactive ones, i.e. they cover a smaller area (figure 6). As already explained previously, this is due to an enhancement of the shielding effect, a phenomenon in which a finger ahead of its neighbouring fingers shields them from further growth (Nagatsu *et al.* 2007; Nagatsu & De Wit 2011). On the other hand, for the lowest
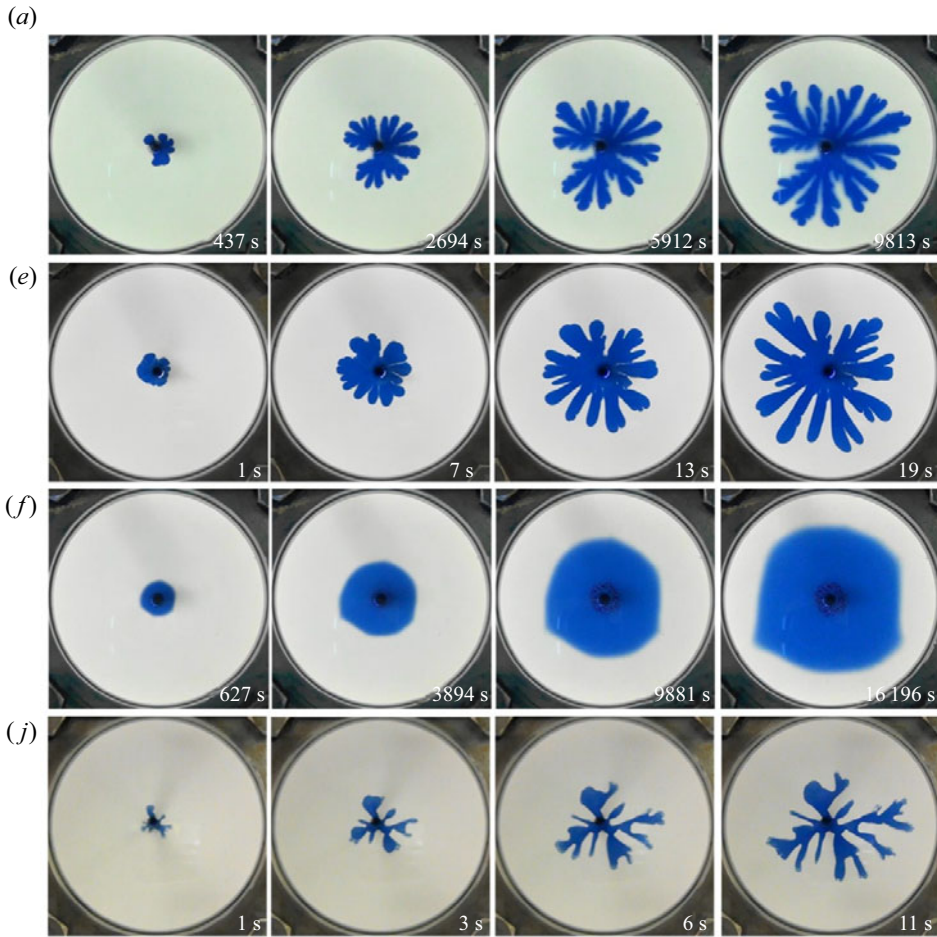
Figure 7. Temporal evolution of the displacement patterns (a,e) non-reactive and (f,j) reactive in figure 4. Pictures of each row are taken at $r = 0.2r_{HS}$, $r = 0.4r_{HS}$, $r = 0.6r_{HS}$ and $r = 0.8r_{HS}$, respectively. This corresponds to different times depending on the conditions as seen on the value of the time inserted in the lower right corner of each panel.

flow rate, the reactive displacement pattern is almost circular and the area density is closer to one.

As will be explained thanks to the numerical part, this stabilisation of VF at lower Pe is due to the fact that, diffusion gaining increased efficiency with regard to advection, the reactants A and B diffuse more into each other generating more of the less-viscous product C (Shukla & De Wit 2020). As the reaction decreases the viscosity in a larger zone, the underlying viscosity gradient decreases, which further favours the passage of the injected less-viscous solution. This explains the filling of the reactive pattern at its centre when Pe decreases and the VF stabilises.

3.2. *Quantitative characterisation of the experimental patterns*

To quantitatively analyse the VF patterns, we measure the area density, d_{area}, defined as the ratio of the area of the fingered pattern to the area πr_{max}^2 of the circle of radius r_{max} passing
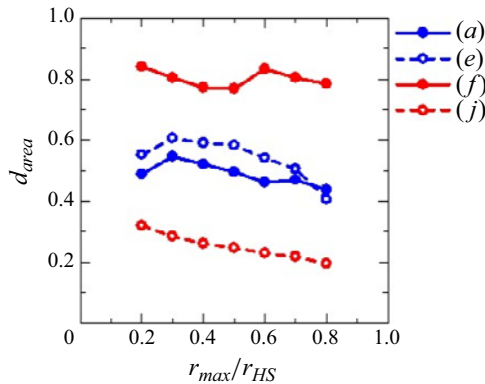
1001 A25-10

Figure 8. Area density as a function of r_{max}/r_{HS} for (a,e,f,j) in figure 7.

at the end of the longest finger (Nagatsu *et al.* 2007). An example of r_{max} is indicated in figure 4(f). The dependence of d_{area} on the flow rate for both non-reactive and reactive cases of figure 4 is shown in figure 6. For low q, d_{area} is larger for the reactive case which is coherent with the observation on figure 4 that the fingered non-reactive pattern is indeed replaced by an almost circular filled circle in the presence of reaction. The reverse is seen for high q: d_{area} is smaller in the reactive case because the shielding effect is enhanced by the reaction and the fingers are much thinner than in the non-reactive situation. The chemical reaction has thus an opposite effect on the VF pattern depending on the flow rate. This conclusion holds all along the temporal evolution of the pattern. Indeed, as seen on figure 7, patterns grow maintaining a similar shape all along their progression. Their area density d_{area} typically decreases with r_{max} for all conditions analysed here (figure 8) such that, at all time, d_{area} in the reactive system is larger than that in the non-reactive system at low q whereas the opposite is seen at high q.

3.3. *Numerical simulations*

To consider the same situation as in the experimental study described above, we perform numerical simulations varying *Pe* both without and with chemical reaction for $R_b = 2$ and analyse the VF pattern by following the dye distribution (Nagatsu & De Wit 2011). In the reactive case, D_a is changed to satisfy the condition $Pe \cdot D_a = 8000$ and we take $R_c = 0$ to consider a reaction decreasing viscosity but keeping the viscosity profile monotonic (Nagatsu & De Wit 2011). In the case without reaction, $D_a = 0$. We set the initial concentration of A to be 10 times larger than that of B because, in experiments, the concentration of the displacing HCl solution, $C_{HCl} = 0.20$ M is about 10 times larger than that of the displaced SPA solution ($C_{SPA} = 0.0133$ M). We analyse the effect of differential diffusivity by either imposing all diffusion coefficients to be the same ($\delta_A = \delta_E = \delta_B = 1 = 1$) as in previous numerical studies on reactive miscible VF (Hejazi & Azaiez 2010; Hejazi *et al.* 2010; Nagatsu & De Wit 2011; Omori & Nagatsu 2020; Shukla & De Wit 2020) or taking the diffusion coefficients of the low-molecular-weight chemical species (i.e. A and the dye E) to be 10 times larger than that of the polymer B, i.e. $\delta_A = \delta_E = 10, \delta_B = 1$.

We first investigate the effect of varying the Péclet number *Pe* on the VF dynamics for the non-reactive case with different diffusivities. Figure 9 shows that fingers become longer and narrower when Pe is increased, which is consistent with the well-known observation that increasing displacement speed makes the interface more unstable to VF
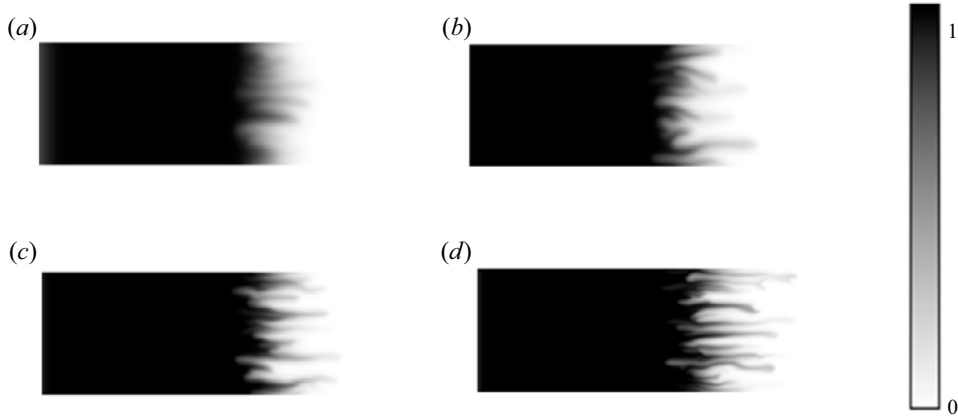
Figure 9. Non-reactive VF patterns shown at time $t = 1$ for different values of the Péclet number: (*a*) $Pe = 1000$, (*b*) $Pe = 2000$, (*c*) $Pe = 4000$ and (*d*) $Pe = 8000$ for different diffusivities ($\delta_A = \delta_E = 10$, $\delta_B = 1$). The grey scale shows the non-dimensional concentration of the dye, E.
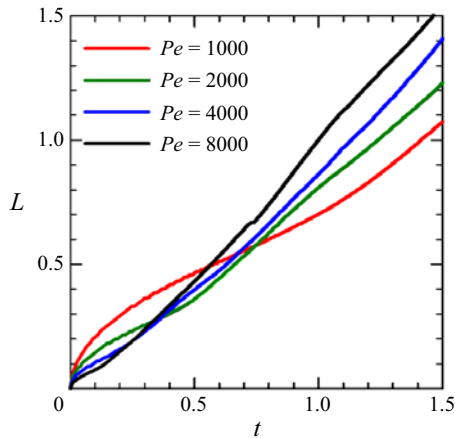

Figure 10. Temporal evolution of the mixing length for the simulations of figure 9. The curves show the average of five simulations with different initial perturbations.

(Chen 1987; Petitjeans *et al.* 1999; Nagatsu & Ueda 2004; Pramanik & Mishra 2015; Suzuki *et al.* 2020). To be more quantitative, we compute the corresponding mixing length L defined here as the length of the zone in which the transverse-averaged concentration of the dye $\bar{e}(x, t)$ lies in the range $0.01 < \bar{e}(x, t) < 0.99$ (Tan & Homsy 1988; Nagatsu & De Wit 2011). Classically, the mixing length L first grows as $\sqrt{t}$ in the early diffusive regime, followed by a linear growth when convection develops. Figure 10 shows that the onset time of VF becomes smaller while the slope of the linear growth increases when Pe increases. This confirms that the non-reactive VF dynamics becomes more unstable as Pe is larger. Note that the fingers narrowing is not observed in the experiment when Pe increases because experimental shear thinning effects not taken into account in the simulations come into play to maintain similar form of the fingers as explained above.

We next investigate the effect of the chemical reaction on the VF dynamics for both different or equal diffusivities at low Pe (figure 11) and high Pe (figure 12). First, panels (*a,c*) of these figures compare the dye distribution in the non-reactive cases. Beyond the
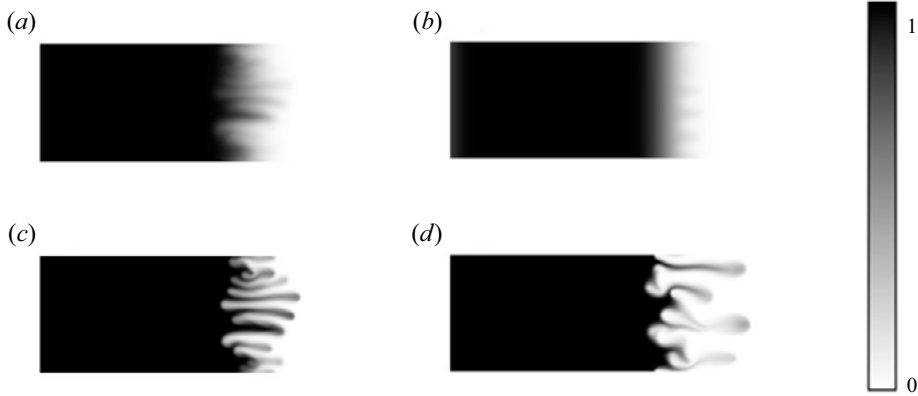
Figure 11. Comparison of non-reactive ($D_a = 0$, first column) and reactive VF ($D_a = 8$, second column) patterns at time $t = 1$ for $Pe = 1000$ with (a)(b) different ($\delta_A = \delta_E = 10$, $\delta_b = 1$) or (c)(d) same diffusivity ($\delta_A = \delta_E = 1$, $\delta_b = 1$). The grey scale shows the non-dimensional concentration of the dye, E.
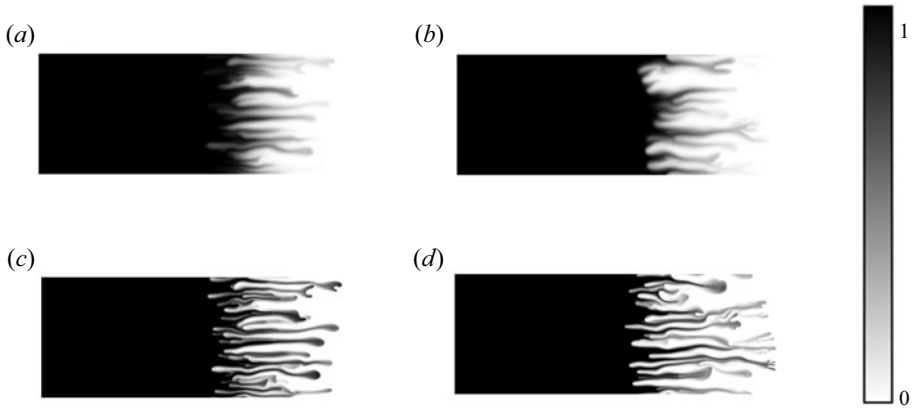

Figure 12. Same as figure 11 for $Pe = 8000$.

fact that the displacement is more unstable when Pe increases, we see that, for both Pe values scanned, the case with differential diffusion (panels a) looks more stable. The underlying fingering pattern is the same, however it appears more blurry and hence more stable if the dye diffuses quickly, because its spatial distribution is then more smoothed out. When inspecting the effect of reaction (panels b,d), we see in figure 11 that the VF pattern for the reactive case at low Pe is more stable than that for the non-reactive case in the different diffusivity case (shown in the upper line panel), which is consistent with the experimental result of figure 4. In figure 11(d), the reactive VF pattern seems also less dense than the non-reactive VF pattern (figure 11c), which is not observed in the experiments. At high Pe (figure 12), in contrast, reactive fingers with $D_a = 1$, shown in the right column, always look more extended and thinner (smaller d_{area}), than those with $D_a = 0$ (left column), which is similar to what is seen in experiments. This conclusion holds whether the diffusivities are the same or not.

The corresponding temporal evolution of the mixing length is shown in figures 13 and 14, respectively. Figure 13 shows that, in the reactive case, the onset time is larger and the slope of the linear growth smaller than in the non-reactive case for different diffusivity
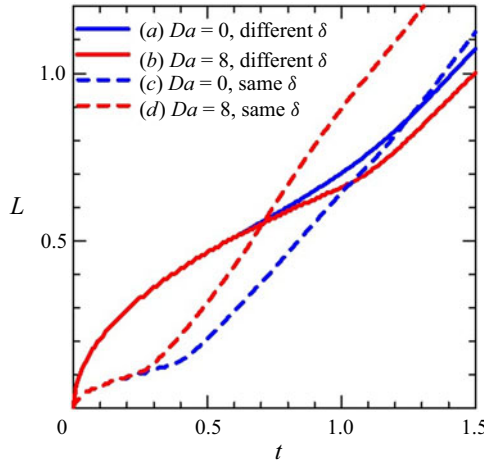
Figure 13. Mixing length of non-reactive ($D_a = 0$) and reactive VF ($D_a = 8$) patterns for $Pe = 1000$ with different ($\delta_A = \delta_E = 10$, $\delta_b = 1$, solid lines) or same diffusivity ($\delta_A = \delta_E = 1$, $\delta_b = 1$, dashed lines). The curves show the average of five data with different initial perturbations.
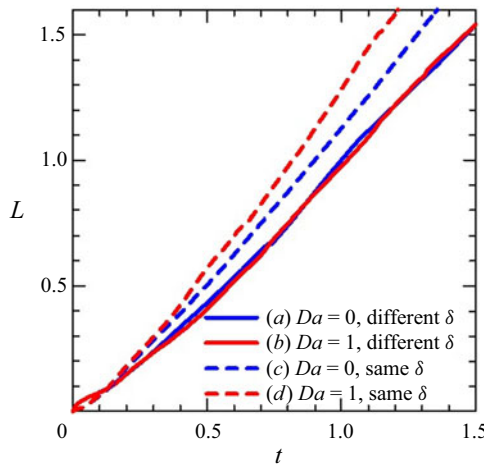

Figure 14. Same as figure 13 for $Pe = 8000$.

while the reverse is seen if diffusion coefficients are equal. These results quantitatively demonstrate that the reaction stabilises the VF instability for low Pe in the differential diffusivity case only. At higher Pe (figure 14), there is no clear difference in the onset time between the reactive and non-reactive system at both different and same diffusivity. For the period of nonlinear growth of VF (when $t > 0.5$), we can see that L in the reactive system is larger than that in the non-reactive system for the same diffusivity, whereas L in the reactive system is almost the same as that in the non-reactive system for different diffusivity. This result for the same diffusivity is consistent with the observation in figure 12(c,d) in which the patterns in the reactive systems look more extended and thinner.
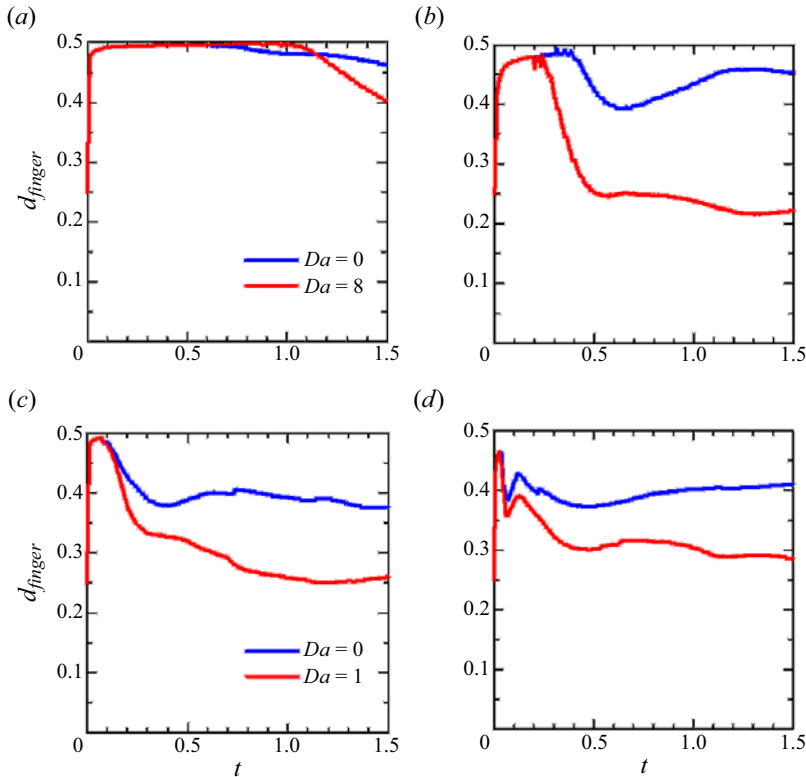
1001 A25-14

Figure 15. Temporal evolution of finger density, d_{finger} comparing non-reactive ($D_a = 0$) and reactive ($D_a \neq 0$) VF for $Pe = 1000$ (upper panel) or $Pe = 8000$ (lower panel) for (a,c) different diffusivities ($\delta_A = \delta_E = 10$, $\delta_b = 1$) or (b,d) same diffusivities ($\delta_A = \delta_E = 1$, $\delta_b = 1$). The curves show the average of five simulations with different initial perturbations.

To further analyse the numerical patterns quantitatively, we compute as well the finger density as

$$d_{finger} = \frac{1}{L_y \times L} \int_0^{L_y} \int_{L_-}^{L_+} e(x, y, t) \, dx \, dy, \qquad (3.1)$$

where $L = L_- + L_+$ and L_- is the length of the upstream finger propagating in the backwards direction with respect to the initial interface while L_+ is the length of the downstream finger propagating in the forwards direction (Nagatsu & De Wit 2011). The temporal evolution of d_{finger} is shown in figure 15. At low Pe, d_{finger} for $D_a = 8$ is larger than that for $D_a = 0$ with different diffusivities as long as t is smaller than around 1.2, which confirms the quantitative observation made in figures 11(a) and 11(b). However, at later time, d_{finger} for $D_a = 8$ becomes smaller than that for $D_a = 0$ (figure 15a). This point is discussed in detail below. With same diffusivities, d_{finger} for $D_a = 0$ is in contrast, larger than that for $D_a = 8$, which confirms the quantitative observation made in figure 11(c,d). For high Pe, d_{finger} for $D_a = 0$ is larger than that for $Da = 1$ no matter whether the diffusivities are the same (figure 15d) or not (figure 15c), which is similar to the quantitative observation made in figure 12. Figure 16 shows d_{finger} at $t = 1$ for various Pe in the case involving different diffusivities. Although the d_{finger} value for the reactive case is smaller than that for the non-reactive case at high Pe, the reverse is seen at low Pe.
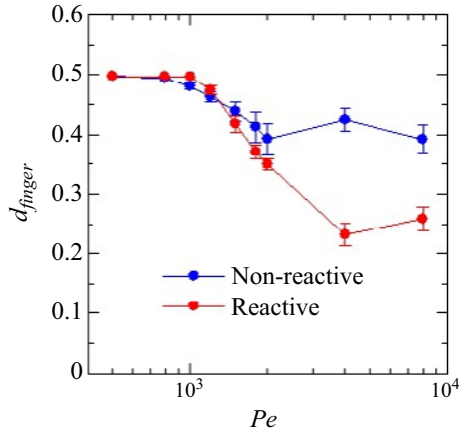
Figure 16. Finger density d_{finger} computed at time $t = 1$ as a function of Pe in the case involving different diffusivities. Each value is the average of five simulations with different initial perturbations with the error bar showing the standard deviation.

This trend is exactly the same as in the experimental results shown in figure 6. Note that at $Pe = 1000$ and 1200, the finger density with error bars is larger in the reactive case. This shows that there is a significant difference between the reactive and non-reactive cases even if the difference is small. To conclude, we see that opposite effects of the reaction on d_{finger} at low and high values of Pe are obtained numerically only when the diffusion coefficients are different.

3.4. *One-dimensional reaction–diffusion profile*

To understand the specific effect of differential diffusivity, we reconstruct viscosity profiles on the basis of one-dimensional reaction–diffusion (RD) concentration profiles, solutions of ((2.11)–(2.13)) in which the injection speed is set to zero:

$$\frac{\partial a}{\partial t} = \frac{\delta_A}{Pe}\nabla^2 a - D_a ab, \tag{3.2}$$

$$\frac{\partial b}{\partial t} = \frac{\delta_B}{Pe}\nabla^2 b - D_a ab, \tag{3.3}$$

$$\frac{\partial c}{\partial t} = \frac{1}{Pe}\nabla^2 c + D_a ab. \tag{3.4}$$

We numerically solve the RD equations (3.2)–(3.4) by an Euler method for time integration with a time interval $dt = 10^{-5}$ and a second-order central difference method with spatial step $dx = 0.005$ to solve the second spatial derivative. The initial condition is $a = 10$, $b = 0$, $c = 0$ for $x - x_0 < 0$ and $a = 0$, $b = 1$, $c = 0$ for $x - x_0 > 0$. No flux boundary conditions are applied at both ends for all concentrations. We obtain the concentration profiles shown in figure 17 for $Pe = 1000$ and $t = 0.5$.

The viscosity profiles of figure 18 are calculated from these concentration profiles using (2.15). The Δ value is the gradient of $\ln\mu$ around $\ln\mu = 1$. First, we see that, for all viscosity profiles, the reactive curve is to the right of the non-reactive one, which is due to the fact that the reactant A is 10 times more concentrated than reactant B (figure 17). The flux of A is thus higher than that of B towards the reaction zone and the $A + B \rightarrow C$ front invades the reactant B and replaces it by C in its wake (figure 17a,c) (Gálfi & Rácz 1988;
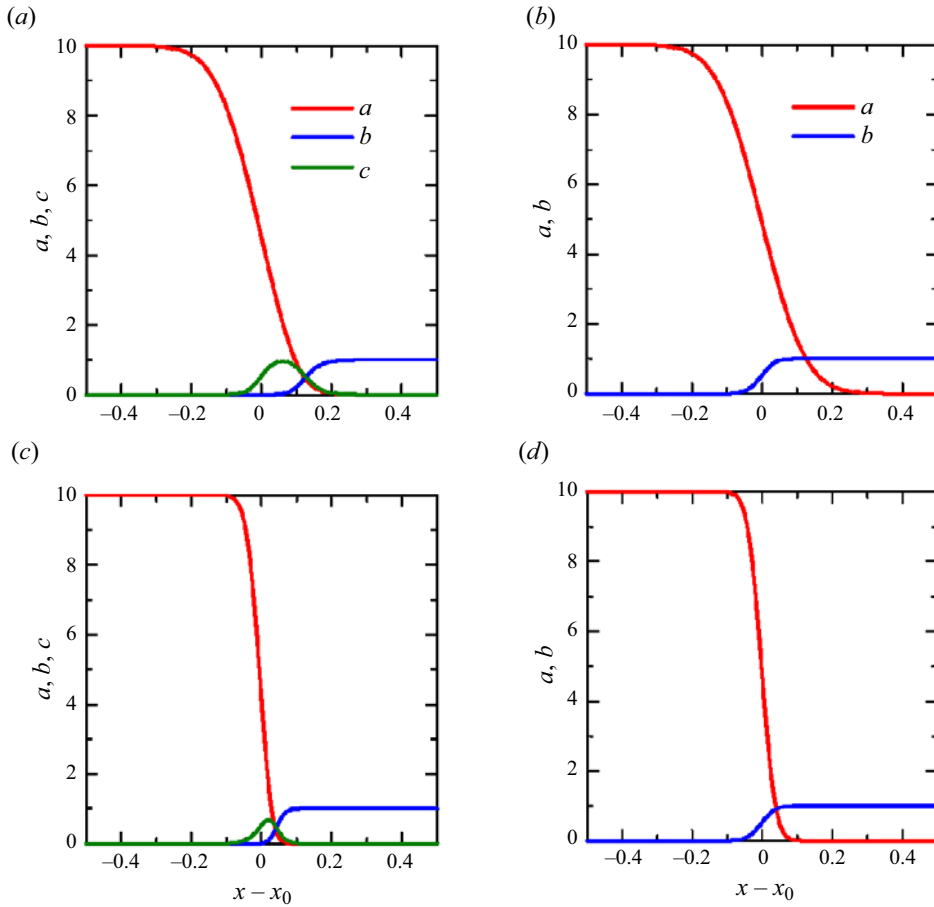
1001 A25-16

Figure 17. Concentration profiles at time $t = 0.5$ for $Pe = 1000$ and (*a*) $(D_a, \delta_A) = (8, 10)$; (*b*) $(D_a, \delta_A) = (0, 10)$; (*c*) $(D_a, \delta_A) = (8, 1)$; and (*d*) $(D_a, \delta_A) = (0, 1)$. Here x_0 represents the position at initial interface. (*a*) Reactive case with $\delta_A = 10$, (*b*) Nonreactive case with $\delta_A = 10$, (*c*) Reactive case with $\delta_A = 1$ and (*d*) Nonreactive case with $\delta_A = 1$.

Gérard & De Wit 2009). This invasion effect is stronger at lower *Pe* as diffusion then has more time to operate. In addition, increasing the Péclet number induces sharper viscosity profiles as seen by comparing the slopes Δ of the curves in the upper panels (low *Pe*) with those of the lower panels (high *Pe*) in figure 18. Again, this is logical as diffusion is more effective in smoothening gradients at lower Péclet numbers.

As the product *C* of the reaction has the same viscosity as the reactant *A* in the simulation ($R_c = 0$), the viscosity is decreased where *B* has been consumed. If *A* diffuses at the same rate than *B* (figure 17*c,d*), this sharpens the viscosity profile as shown in the right column of figure 18. In contrast, if *A* diffuses 10 times faster than *B* (figure 17*a,b* and left column of figure 18), the reaction front invades and consumes *B* even faster, more *C* is produced (figure 17*a*), and the gradient of viscosity decreases (figure 18*a,c*). This suggests that stabilisation of VF at lower values of *Pe* is here due to the efficiency of the fast diffusion of the reactant *A* (HCl in the experiment) into the slower diffusing polymer to reduce locally the viscosity gradient in the reactive zone.
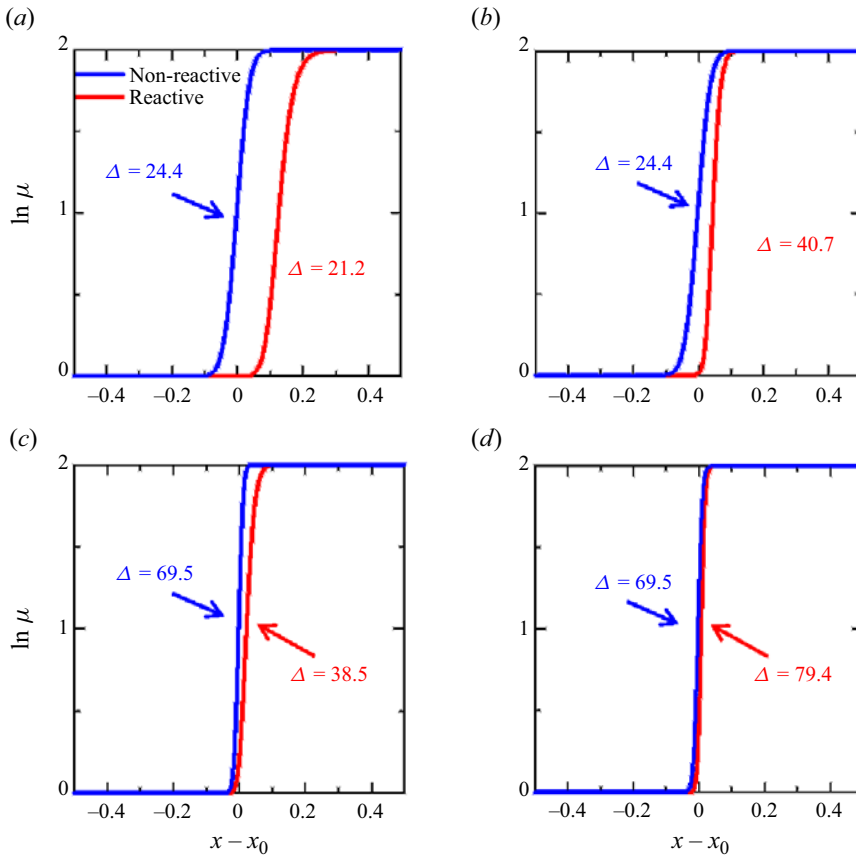
Figure 18. Viscosity profiles at time $t = 0.5$ for the non-reactive case $D_a = 0$ (blue curves) and reactive case $D_a = 8$ (red curves) for $Pe = 1000$ (upper line) or $D_a = 1$ for $Pe = 8000$ (lower line) and (a,c) $\delta_A = 10$ (b,d) $\delta_A = 1$: (a) $Pe = 1000$, different δ, (b) $Pe = 1000$, same δ, (c) $Pe = 8000$, different δ and (d) $Pe = 8000$, same δ. The other parameters are $R_b = 2$, $R_c = 0$, $a_0 = 10$, $b_0 = 1$ and $\delta_B = 1$.

At higher *Pe*, this mechanism seems less efficient because the nonlinear enhancement of the shielding effect triggered by advection wins over the diffusive effects, which explains the formation of a less-dense pattern in the reactive case, as already explained in Nagatsu *et al.* (2007).

We find that the fact that the reactive case with different diffusivities is more stable than the non-reactive case for low *Pe*, has a time dependency. Looking closely at d_{finger} in figure 15(a), we see that d_{finger} for the reactive case is larger than that for the non-reactive case until roughly $t = 1.2$. After $t = 1.2$, the reverse result is observed. This suggests that the stabilising effect of VF by reactions might depend on time. Figure 19 shows the viscosity profiles and the numerical VF results at $t = 1.5$. Comparing the (b) non-reactive and (c) reactive cases with different diffusivity, we find that the non-reactive case seems more stable than the reactive case, while we see the reverse at $t = 1.0$ (figure 11). Moreover, the Δ value for the reactive case is steeper than that for the non-reactive case, which implies increased destabilisation by reaction. These results are consistent with the d_{finger} results in figure 15(a) in which d_{finger} becomes smaller in the reactive case at later times.
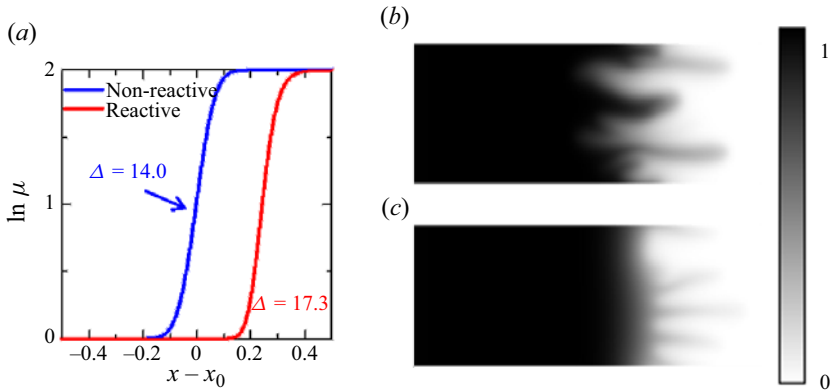
1001 A25-18

Figure 19. (*a*) Viscosity profile at $t = 1.5$ and numerical VF results for (*b*) non-reactive ($D_a = 0$) and (*c*) reactive ($D_a = 8$) cases. The parameters for (*b*) and (*c*) are: $Pe = 1000$, $R_b = 2$, $R_c = 0$, $a_0 = 10$, $b_0 = 1$, $\delta_A = \delta_E = 10$ and $\delta_B = 1$. The grey scale shows the non-dimensional concentration of the dye, E.

3.5. *Remarks on the value of R_b, R_c and D_a for the experiment*

Let us here discuss the values of R_b, R_c and D_a for the experiments. Regarding R_b, because of the radial geometry and the shear thinning viscosity of the more-viscous fluid, the apparent viscosity contrast between reactants varies with the flow rate and time (the apparent displacement velocity decreases with radius at a constant injection rate in the radial geometry). The value of R_b when r_{max} varies from 2 to 47 mm is calculated to be $8.0 < R_b < 9.9$ for the lowest flow rate and $3.9 < R_b < 5.9$ for the highest flow rate. The value of R_b used in the simulations is lower to avoid numerical stiffness. However, we emphasise that the quantitative matching of the value of R_b is not important in the present study to elucidate the mechanism behind the experimental results. The details of the calculations of R_b for experiments are provided in Appendix A. The viscosity measurement results (figure 2) show that the viscosity of the product solution is approximately equal to that of water. This indicates that we can consider that $R_c = 0$. In the experiment, D_a cannot be calculated because the reaction occurs instantaneously. We note that the calculation method for infinite D_a reported in Nagatsu & De Wit (2011) cannot be used when the diffusion coefficients are different. Therefore, the present study, in which the effect of differential diffusion is highlighted, performs simulations for finite values of D_a.

4. Conclusions

The present study has experimentally and numerically investigated the influence of varying the injection flow rate on reactive miscible VF in the case of a chemical reaction decreasing the viscosity of the solutions *in situ* for monotonic viscosity profiles. At large flow rates, i.e. large *Pe*, we recover experimental results from Nagatsu *et al.* (2007) and corresponding numerical results from Nagatsu & De Wit (2011) showing that the reactive VF pattern covers a smaller area than its non-reactive equivalent, a change due to an increase of the shielding effect when the viscosity is decreased by the reaction. We experimentally find that opposite effects of the reaction on the VF pattern are obtained at lower values of *Pe*. Indeed, at low flow rates, the reaction stabilises the VF dynamics, creating fingered patterns covering a larger area. At the lowest value of *Pe* scanned here, we even observe a large stabilisation with resulting circular displacements. Simulations in

which the diffusivity of the injected reactant *A* is larger than that of the displaced reactant *B* and of the product *C* can reproduce the same stabilising trend as in the experiment. Quantitative analysis of the dynamics shows that low *Pe* values and faster diffusion of the invading reactant allow a more effective decrease of the viscosity *in situ* and, hence, a better stabilisation of VF. One-dimensional viscosity profiles reconstructed on the basis of a RD model confirm that an efficient decrease in the viscosity gradient needed for VF stabilisation is obtained only in the reactive case with different diffusivities. Further studies will be undertaken to optimise the stabilisation conditions of VF by such chemical reactions.

Declaration of interests. The authors report no conflict of interest.

Author ORCIDs.
- R.X. Suzuki https://orcid.org/0000-0001-5386-4222;
- Y. Nagatsu https://orcid.org/0000-0003-2203-9830;
- A. De Wit https://orcid.org/0000-0002-3231-0906.

Appendix A. Calculation of R_b in the experiments

In experiments, the value of R_b varies with flow rate and time. Indeed, the viscosity of the displaced shear-thinning polymer solution varies with the shear rate, which is itself a function of the radius from injection point. To compute R_b, we first calculate the shear rate $\dot{\gamma}$ as (Nagatsu *et al.* 2007)

$$\dot{\gamma} = \frac{q}{\pi r b^2}. \tag{A1}$$

Then, we calculate the viscosity $\eta_{polymer}$ of the polymer (0.125 wt %) SPA solution for each calculated $\dot{\gamma}$. Finally, the R_b value is computed as

$$R_b = \ln\left(\frac{\eta_{polymer}}{\eta_{water}}\right), \tag{A2}$$

where η_{water} is the viscosity of water (1.0 mPa·s). We find that the value of R_b when r_{max} varies from 2 to 47 mm is $8.0 < R_b < 9.9$ for the lowest flow rate and $3.9 < R_b < 5.9$ for the highest flow rate.

Appendix B. How to measure the finger width

The r_{max} is radius of the longest finger in figure 20. Then, the finger width is measured at $0.8r_{max}$ shown as a red circle in figure 20. The average finger width $\langle w \rangle$ is defined as the total length of the red curve covering black fingers divided by the number of fingers.
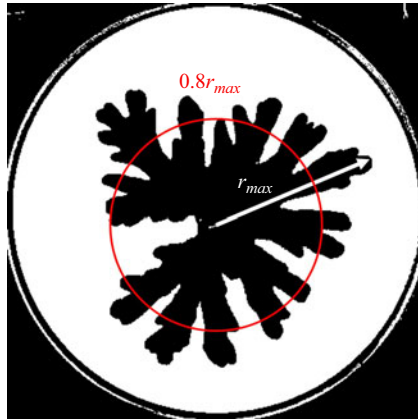
Figure 20. How to measure the finger width at an arbitrary time.

REFERENCES

BERG, S. & OTT, H. 2012 Stability of CO_2-brine immiscible displacement. *Intl J. Greenh. Gas Control* **11**, 188–203.

BHASKAR, K.R., GRIK, P., TURNER, B.S., BRADLEY, J.D., BANSIL, R., STANLEY, H.E. & LAMONT, J.T. 1992 Viscous fingering of HCl through gastric mucin. *Nature* **360**, 458–461.

BISCHOFBERGER, I., RAMACHANDRAN, R. & NAGEL, S.R. 2014 Fingering versus stability in the limit of zero interfacial tension. *Nat. Commun.* **5**, 5265.

BONN, D., KELLAY, H., BEN AMAR, M. & MEUNIER, J. 1995 Viscous finger widening with surfactants and polymers. *Phys. Rev. Lett.* **75**, 2132–2135.

BROYLES, B.S., SHALLIKER, R.A., CHERRAK, D.E. & GUIOCHON, G. 1998 Visualization of viscous fingering in chromatographic columns. *J. Chromatogr.* A **822**, 173–187.

BUNTON, P., TULLIER, M., MEIBURG, E. & POJMAN, J. 2017 The effect of a crosslinking chemical reaction on pattern formation in viscous fingering of miscible fluids in a Hele-Shaw cell. *Chaos* **27**, 104614.

CHEN, J.D. 1987 Radial viscous fingering patterns in Hele-Shaw cells. *Exp. Fluids* **5**, 363–371.

DE WIT, A. 2016 Chemo-hydrodynamic patterns in porous media. *Phil. Trans. R. Soc.* A **374**, 20150419.

DE WIT, A. 2020 Chemo-hydrodynamic patterns and instabilities. *Annu. Rev. Fluid Mech.* **52**, 531–555.

DE WIT, A. & HOMSY, G.M. 1999 Nonlinear interactions of chemical reactions and viscous fingering in porous media. *Phys. Fluids* **11**, 949–951.

ENGELBERTS, W.F. & KLINKENBERG, L.J. 1951 Laboratory experiments on displacement of oil by water from rocks of granular materials. *Proc. 3rd World Pet. Cong. II*, 544–554.

ESCALA, D.M., DE WIT, A., CARBALLIDO-LANDEIRA, J. & MUNUZURI, A.P. 2019 Viscous fingering induced by a pH-sensitive clock reaction. *Langmuir* **35**, 4182–4188.

ESCALA, D.M. & MUNUZURI, A.P. 2021 A bottom-up approach to construct or deconstruct a fluid instability. *Sci. Rep.* **11**, 24368.

FERNANDEZ, J. & HOMSY, G.M. 2003 Viscous fingering with chemical reaction: effect of in-situ production of surfactants. *J. Fluid Mech.* **480**, 267–281.

GÁLFI, L. & RÁCZ, Z. 1988 Properties of the reaction front in an $A + B \rightarrow C$ type reaction-diffusion process. *Phys. Rev.* A **38**, 3151–3154(R).

GÉRARD, T. & DE WIT, A. 2009 Miscible viscous fingering induced by a simple $A + B \rightarrow C$ chemical reaction. *Phys. Rev.* E **79**, 016308.

HAUDIN, F., CALLEWAERT, M., DE MALSCHE, W. & DE WIT, A. 2016 Influence of nonideal mixing properties on viscous fingering in micropillar array columns. *Phys. Rev. Fluids* **1**, 074001.

HAUDIN, F. & DE WIT, A. 2015 Patterns due to an interplay between viscous and precipitation-driven fingering. *Phys. Fluids* **27**, 113101.

HEJAZI, S.H. & AZAIEZ, J. 2010 Non-linear interactions of dynamic reactive interfaces in porous media. *Chem. Engng Sci.* **65**, 938–949.

HEJAZI, S.H., TREVELYAN, P.M.J., AZAIEZ, J. & DE WIT, A. 2010 Viscous fingering of a miscible reactive $A + B \rightarrow C$ interface: a linear stability analysis. *J. Fluid Mech.* **652**, 501–528.

HOMSY, G.M. 1987 Viscous fingering in porous media. *Ann. Rev. Fluid Mech.* **19**, 271–311.

KAWAGUCHI, M. 2001 Viscous fingering in polymeric systems. *Nonlinear Anal.* **47**, 907–918.

KEABLE, D., JONES, A., KREVOR, S., MUGGERIDGE, A. & JACKSON, S.J. 2022 The effect of viscosity ratio and Péclet number on miscible viscous fingering in a Hele-Shaw cell: a combined numerical and experimental study. *Transp. Porous Med.* **143**, 23–45.

KIM, M.C., PRAMANIK, S., SHARMA, V. & MISHRA, M. 2021 Unstable miscible displacements in radial flow with chemical reactions. *J. Fluid Mech.* **917**, A25.

LAJEUNESSE, E., MARTIN, J., RAKOTOMALALA, N. & SALIN, D. 1997 3D instability of miscible displacements in a Hele-Shaw cell. *Phys. Rev. Lett.* **79**, 5254–5257.

LAKE, L.W., JOHNS, R.T., ROSSEN, W.R. & POPE, G.A. 2014 *Fundamentals of Enhanced Oil Recovery*. Society of Petroleum Engineers.

MCCLOUD, K.V. & MAHER, J.V. 1995 Experimental perturbations to Saffman–Taylor flow. *Phys. Rep.* **260**, 139–185.

MISHRA, M., TREVELYAN, P.M.J., ALMARCHA, C. & DE WIT, A. 2010 Influence of double diffusive effects on miscible viscous fingering. *Phys. Rev. Lett.* **105**, 204501.

NAGATSU, Y. 2015 Viscous fingering phenomena with chemical reactions. *Curr. Phys. Chem.* **5**, 52–63.

NAGATSU, Y., BAE, S.K., KATO, Y. & TADA, Y. 2008 Miscible viscous fingering with a chemical reaction involving precipitation. *Phys. Rev. E* **77**, 067302.

NAGATSU, Y. & DE WIT, A. 2011 Viscous fingering of a miscible reactive $A + B \rightarrow C$ interface for an infinitely fast chemical reaction: nonlinear simulations. *Phys. Fluids* **23**, 043103.

NAGATSU, Y., IGUCHI, C., MATSUDA, K., KATO, Y. & TADA, Y. 2010 Miscible viscous fingering involving viscosity changes of the displacing fluid by chemical reactions. *Phys. Fluids* **22**, 024101.

NAGATSU, Y., ISHII, Y., TADA, Y. & DE WIT, A. 2014 Hydrodynamic fingering instability induced by a precipitation reaction. *Phys. Rev. Lett.* **113**, 114501.

NAGATSU, Y., KONDO, Y., KATO, Y. & TADA, Y. 2009 Effects of moderate Damköhler number on miscible viscous fingering involving viscosity decrease due to a chemical reaction. *J. Fluid Mech.* **625**, 97–124.

NAGATSU, Y., KONDO, Y., KATO, Y. & TADA, Y. 2011 Miscible viscous fingering involving viscosity increase by a chemical reaction with moderate Damköhler number. *Phys. Fluids* **23**, 014109.

NAGATSU, Y., MATSUDA, K., KATO, Y. & TADA, Y. 2007 Experimental study on miscible viscous fingering involving viscosity changes induced by variations in chemical species concentrations due to chemical reactions. *J. Fluid Mech.* **571**, 475–493.

NAGATSU, Y. & UEDA, T. 2004 Analytical study of effects of finger-growth velocity on reaction characteristics of reactive miscible viscous fingering by using a convection-diffusion-reaction model. *Chem. Engng Sci.* **59**, 3817–3826.

NITTMAN, J., DACCORD, G. & STANLEY, H. 1985 Fractal growth of viscous fingers: quantitative characterization of a fluid instability phenomenon. *Nature* **314**, 141–144.

OMORI, K. & NAGATSU, Y. 2020 Numerical simulations of miscible viscous fingering involving viscosity changes of the displacing fluid by $A + B \rightarrow C$ chemical reactions. *AIP Adv.* **10**, 095014.

PATERSON, L. 1985 Fingering with miscible fluids in a Hele-Shaw cell. *Phys. Fluids* **28**, 26–30.

PETITJEANS, P., CHEN, C.Y., MEIBURG, E. & MAXWORTHY, T. 1999 Miscible quarter five-spot displacements in a Hele-Shaw cell and the role of flow-induced dispersion. *Phys. Fluids* **11**, 1705–1716.

PODGORSKI, T., SOSTARECZ, M.C., ZORMAN, S. & BELMONTE, A. 2007 Fingering instabilities of a reactive micellar interface. *Phys. Rev. E* **76**, 016202.

PRAMANIK, S. & MISHRA, M. 2015 Effect of Péclet number on miscible rectilinear displacement in a Hele-Shaw cell. *Phys. Rev. E* **91**, 033006.

RIOLFO, L.A., NAGATSU, Y., IWATA, S., MAES, R., TREVELYAN, P.M.J. & DE WIT, A. 2012 Experimental evidence of reaction-driven miscible viscous fingering. *Phys. Rev. E* **85**, 015304(R).

SABET, N., MOHAMMADI, M., ZIRAHI, A., ZIRRAHI, M., HASSANZADEH, H. & ABEDI, J. 2020 Numerical modeling of viscous fingering during miscible displacement of oil by a paraffinic solvent in the presence of asphaltene precipitation and deposition. *Intl J. Heat Mass Transfer* **154**, 119688.

SAFFMAN, P.G. & TAYLOR, G.I. 1958 The penetration of a fluid into a porous medium or Hele-Shaw cell containing a more viscous liquid. *Proc. R. Soc. Lond.* A **245**, 312–329.

SHARMA, V., PRAMANIK, S., CHEN, C.-Y. & MISHRA, M. 2019 A numerical study on reaction-induced radial fingering instability. *J. Fluid Mech.* **862**, 624–638.

SHUKLA, P. & DE WIT, A. 2016 Fingering dynamics driven by a precipitation reaction: nonlinear simulations. *Phys. Rev. E* **93**, 023103.

SHUKLA, P. & DE WIT, A. 2020 Influence of the Péclet number on reactive viscous fingering. *Phys. Rev. Fluids* **5**, 014004.

SINGH, P., LALITHA, R. & MONDAL, S. 2021 Saffman-Taylor instability in a radial Hele-Shaw cell for a shear-dependent rheological fluid. *J. Non-Newtonian Fluid Mech.* **294**, 104579.

STEWART, S., MARIN, D., TULLIER, M., POJMAN, J., MEIBURG, E. & BUNTON, P. 2018 Stabilization of miscible viscous fingering by a step growth polymerization reaction. *Exp. Fluids* **59**, 114.

SUZUKI, R.X., QUAH, F.W., BAN, T., MISHRA, M. & NAGATSU, Y. 2020 Experimental study of miscible viscous fingering with different effective interfacial tension. *AIP Avd.* **10**, 115219.

TAFUR, N., ESCALA, D.M., SOTO, A. & MUNUZURI, A.P. 2021 Highly viscous fluid displaced by a chemically controlled reactive interface. *Chaos* **31**, 023135.

TAN, C.T. & HOMSY, G.M. 1988 Simulation of nonlinear viscous fingering in miscible displacement. *Phys. Fluids* **31**, 1330–1338.

TSUZUKI, R., BAN, T., FUJIMURA, M. & NAGATSU, Y. 2019 Dual role of surfactant-producing reaction in immiscible viscous fingering evolution. *Phys. Fluids* **31**, 022102.

VERMA, P., SHARMA, V. & MISHRA, M. 2022 Radial viscous fingering induced by an infinitely fast chemical reaction. *J. Fluid Mech.* **945**, A19.

VIDEBAEK, T.E. & NAGEL, S.R. 2019 Diffusion-driven transition between two regimes of viscous fingering. *Phys. Rev. Fluids* **4**, 033902.

ZHAO, H. & MAHER, J.V. 1992 Viscoelastic effects in patterns between miscible liquids. *Phys. Rev.* A **45**, R8328–R8331.